

Measurements of the Growth and Coagulation of Soot Particles in a High-Pressure Shock Tube

H. KELLERER,* R. KOCH, and S. WITTIG

*Lehrstuhl und Institut für Thermische Strömungsmaschinen, Universität Karlsruhe, Kaiserstraße 12,
76128 Karlsruhe, Germany*

The advantage of well-defined experimental conditions in shock tubes has been used to investigate the growth and coagulation of soot particles at high pressures. The measurements have been made for fuel-rich oxidation and pyrolysis of different hydrocarbons behind the reflected shock at pressures between 10 and 60 bar and temperatures between 1500 and 2300 K. In addition to soot volume fraction, time-resolved scattering measurements yielded particle diameters and number densities; all these give insight into both surface growth and coagulation at enhanced pressures. The temperature behind the reflected shock was monitored by two-color pyrometry. Soot growth was characterized by induction periods and soot growth rates. At low final soot yields, the growth rate of soot depends on the square of the carbon concentration. At high soot yields, reduced growth rates of soot volume fraction were observed and can be attributed to a lack of growth species. **At constant carbon concentration no pressure dependence of soot volume fraction could be found.** Particle diameters between 15 and 40 nm were measured. The number density of particles was found to increase strongly with soot volume fraction. Calculated and measured particle number densities agree well during early soot growth. However, at longer times the experiments reveal coagulation rates which are significantly smaller than predicted. This behavior indicates that collisions of deactivated soot particles are characterized by sticking probabilities lower than unity. A correlation for the sticking probability has been established to match both the experimental results and calculations. © 1999 by The Combustion Institute

INTRODUCTION

Minimization of pollutant formation is one of the main targets in the development of future jet engines. The major pollutants are nitrogen oxides and soot. Soot particles emitted in the upper atmosphere are suspected of contributing significantly to the depletion of the ozone layer. However, increased combustion pressures, introduced to raise the thermal efficiency of jet engines, are often accompanied by enhanced soot formation. To obtain a better understanding of soot formation under aircraft engine conditions, more detailed investigations of soot particle growth at elevated pressures are needed.

In most investigations of soot formation, high-pressure laminar premixed flames have been studied [1, 2]. Below 5 bar, soot volume fraction depends on p^2 . At higher pressures, p , soot growth is less sensitive to pressure. With increasing pressure, particle number densities exceed those at atmospheric conditions. Detailed optical measurements of particle growth have been restricted to pressures below 15 bar [3]. Other important contributions come from

experiments in shock tubes. Most studies have focused on pyrolysis and were limited to the determination of the soot volume fraction by simple extinction techniques [4, 5]. The application of scattering methods in shock tubes has been restricted to experiments in the incident shock region, as introduced initially by Graham *et al.* [6] for investigating soot coagulation in the regime of free molecular flows. Recently these methods have been applied to study the morphology of soot aggregates at high temperatures and pressures [7].

To obtain a better understanding of soot formation at higher pressures, soot formation during the pyrolysis and the fuel-rich oxidation of hydrocarbons in a high-pressure shock tube has been intensively investigated [8, 9]. The present study extends that work and reports experiments on the sooting behavior of different hydrocarbons with respect to temperature, pressure, carbon concentration, and stoichiometry. The shock tube technique offers the advantage that these parameters can be changed independently. In addition to extinction, a light scattering technique for particle sizing has been applied in the reflected shock region. It provides the opportunity of studying the growth and

*Corresponding author. E-mail: horst.kellerer@bmw.de

coagulation of soot particles in the transition region between free molecular flow and the continuum regime under well-defined conditions. Information on particle diameters and number densities is important for soot oxidation, and the evaluation of soot emission has great relevance to the atmosphere. In addition, the results allow validation of models of soot production at elevated pressures.

EXPERIMENTAL

Shock Tube Facility

The experiments were done in a conventional shock tube, which has been described in detail [8]. It is 4950 mm in total length with a driven section of 2970 mm. The inner diameter is 31.4 mm. Three windows mounted 10 mm from the end of the driven section allow access for optical measurements. The shock tube is equipped with three piezoelectric pressure transducers to determine the speed of the incident and reflected shocks and also the pressure in the measurement plane. By applying the ideal gas law and the equation of state, the thermodynamic state in the measurement plane can be derived. The experiments were done behind the reflected shock. In order to extend the observation time during the experiments on coagulation, the shock tube was partly operated at overtaiored conditions. The results presented below were obtained for different aliphatic and aromatic hydrocarbons for fuel-rich oxidation and pyrolysis at pressures from 10 to 60 bar and temperatures from 1500 to 2300 K. In this paper, stoichiometry is characterized by the equivalence ratio ϕ . The carbon concentration was changed by varying the partial pressure of the hydrocarbon fuel investigated. Gas mixtures heavily diluted with argon were prepared manometrically using high-purity gases.

Optical Setup

From extinction measurements at 632.8 nm the soot volume fraction was derived by application of the Rayleigh approximation:

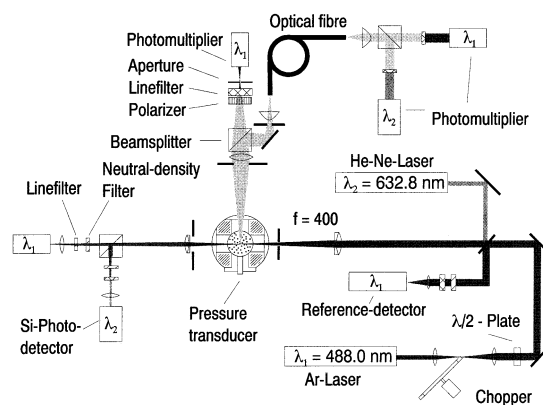


Fig. 1. Optical setup for particle characterization and temperature measurements.

$$f_V = \frac{\ln\left(\frac{I}{I_0}\right) \lambda}{6\pi l} \frac{1}{\text{Im}\left\{\frac{m^2 - 1}{m^2 + 2}\right\}}, \quad (1)$$

where I_0 and I are the beam intensities before and after the shock tube, l is the extinction length, and m the refractive index of the soot particles. The scattering-extinction technique with a scattering angle of 90° enables one to determine soot particle diameters and also number densities. Preliminary experiments revealed that the scattering-extinction technique is more reliable than the commonly used multiwavelength extinction or emission techniques [9].

The optical setup, together with the cross-section of the shock tube, is shown in Fig. 1. The beams of a He-Ne laser operating at 632.8 nm and an Ar laser at 488 nm are superposed and focused on the center of the tube. The polarization of the laser light is rotated by a $\lambda/2$ -plate for VV-scattering. The scattered light is detected at a scattering angle of 90° . It is conditioned by a polarizer and a narrow band interference filter before being focused on a pinhole in front of a photomultiplier tube. To discriminate between scattering and emission from the particles, the beam is modulated by a beam chopper (40 kHz). The laser intensity and beam modulation are monitored by a reference detector, whereas the transmitted light is split up into the two wavelengths and detected by Si photodiodes. The scattering system was calibrated by scattering from argon; the scattered signal has to be

corrected for vacuum scattering caused by reflections from windows and the shock tube's wall.

Based on Mie theory, particle diameters and number densities can be calculated from the intensities of the scattered and transmitted light [10]. Assuming Rayleigh approximation the absorption coefficient k_{ext} and the vertical polarized scattering coefficient Q_{VV} of polydisperse particles can be expressed as:

$$k_{\text{abs}} = -\frac{\pi^2}{\lambda} \text{Im} \left\{ \frac{m^2 - 1}{m^2 + 2} \right\} N \cdot \int_0^{\infty} p(d) d^3 dd \quad (2)$$

$$Q_{VV} = \frac{\pi^4}{4\lambda^4} \left| \frac{m^2 - 1}{m^2 + 2} \right|^2 N \cdot \int_0^{\infty} p(d) d^6 dd \quad (3)$$

Looking at k_{abs} and Q_{VV} , it is obvious that their ratio, which can be obtained from the measurements, is only a function of refractive index, particle size, and the size distribution. If the particle number density is calculated, it is found that $N \sim \langle d^6 \rangle / \langle d^3 \rangle^2$ where $\langle d^i \rangle$ is the i -th moment of the distribution. Hence, in addition to the refractive index, assumptions about the size distribution are required. Primary particles extracted from the shock tube were analyzed by transmission electron microscopy (TEM). The particle distribution was found to match a log-normal distribution with a geometric standard deviation of $\sigma_g = 0.2$.

After careful investigation of values of refractive index in the literature, the real and imaginary parts of the refractive index were calculated according to the dispersion model with constants suggested by Charalampopoulos et al. [11]. The refractive index derived by Lee and Tien [12] was found to require a soot density of 1.0 g/cm^3 to prevent the yield of soot in benzene pyrolysis from rising above a conversion of 100%. This value deviates strongly from the soot densities determined for particles extracted from flames. In addition, the number densities calculated with this refractive index [12] are too high to be explained by coagulation theory.

Due to the interaction of the reflected shock with the boundary layer between the shock and the interface, constant states of pressure and

temperature behind the reflected shock could not be realized. A pressure record for the overtoured case showing an initial rise, followed by almost constant conditions over a time of 3 ms is given below in Fig 6. Similar observations have been made by Tsuboi and Nagaya [13]. As growth rates of soot depend strongly on temperature, time-resolved values of the temperature are important for the analysis of the experimental observations. Temperature boundary conditions are indispensable for simulating particle growth or validating models of soot formation. Therefore, in addition to particle sizing, the particles' temperature during soot growth was monitored by two-color pyrometry. A theoretical analysis proved that radiative losses from the particles can be neglected, so that a particle and its ambient gas have almost identical temperatures. It was found to be necessary to determine the emissivities at both wavelengths by laser absorption, as the gray body assumption or extrapolation of soot's refractive index by common dispersion models can introduce serious errors. This is due to a considerable contribution from polycyclic aromatic hydrocarbons (PAH) to light extinction in the visible under fuel-rich conditions during the initial phase of soot formation. Spectral emissivities were obtained from extinction measurements using $\epsilon(\lambda) = \alpha(\lambda)$. Emissions at the two laser wavelengths were detected by introducing a beam splitter in the scattering optics as shown in Fig. 1. The emitted light was focused on a plastic fiber to guide it to the receiving optics. The system was calibrated with a tungsten strip lamp of known temperature and emissivity.

Data Processing

Typical signals of the transmitted and scattered light are presented in Fig. 2. The extinction of laser light starts with a characteristic delay (induction time) after the passage of the reflected shock; then it increases strongly, but does not reach a constant value during the measurement time. The scattered intensity can be calculated from the difference between the upper and the lower envelopes of the AC signal presented in the lower part of Fig. 2. Comparison of the two signals reveals that there is already some absorption present at the onset of particle scattering. This indicates that absorbing species, which might be precursors of

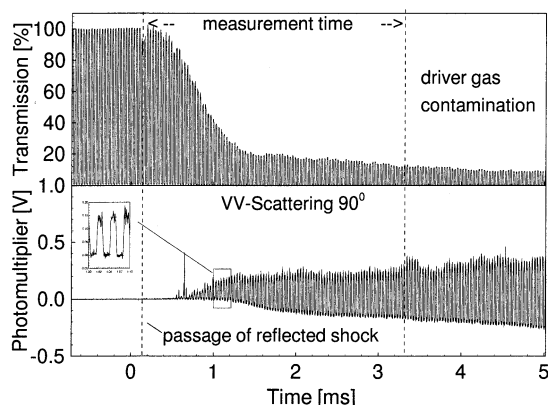


Fig. 2. Transmitted and scattered signals for C_7H_{16} , $\phi = 5$, $Ar = 99.5\%$, $T = 1820\text{ K}$, $p = 59.1\text{ bar}$.

soot are present prior to the appearance of the first particles. Additional extinction measurements performed in the IR demonstrate that absorption decreases with increasing wavelength, confirming the ability of PAH to absorb light at longer wavelengths, while they grow in size. During the measurements, strong scattered signals were partly observed for times longer than 3 ms after the passage of the reflected shock. We attribute this effect to small fragments created by the rupture of the diaphragm and transported by the driver gas. Therefore, measurements were made for only 3 ms.

Reaction temperatures were calculated from the two-color emission and extinction signals. Experiments at high temperature with immediate soot formation after the passage of the reflected shock were used to compare measured and calculated temperatures. Test runs with "old" soot particles from the previous experiment dispersed in argon were carried out, too. In both cases the agreement between the measured and the calculated temperatures directly after the passage of the reflected shock, based on the velocity of the incident and the reflected shock, was better than 2%.

RESULTS

Induction Period and Maximum Soot Growth Rate

The induction period and the soot growth rate were determined from extinction measurements

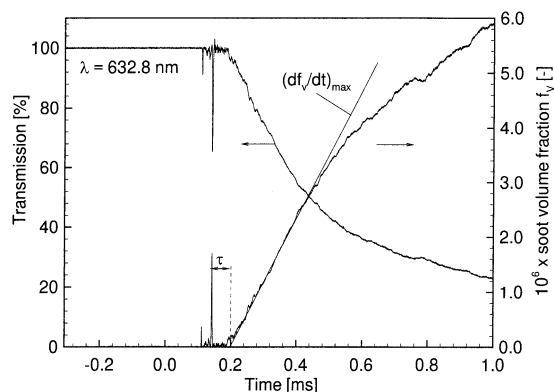


Fig. 3. Transmission and soot volume fraction during measurement time (C_7H_8 , $\phi = 5$, $Ar = 99.5\%$, $p = 30.7\text{ bar}$).

at 632.8 nm. Soot volume fraction was obtained using the Rayleigh approximation. A typical example of a transmission signal and the calculated soot volume fraction is given in Fig. 3. The experiments were carried out for the induction time shorter than the time for the initial pressure and temperature to rise after the reflected shock. The influence of temperature, pressure, carbon concentration, and stoichiometry was investigated.

The induction period τ was determined as the time between the passage of the reflected shock through the measurement plane and the intersection of the tangent at the point of maximum soot growth with the axis (see Fig. 3). It was found that the induction period τ can be represented in the Arrhenius form:

$$1/\tau = A \cdot [C]^n \cdot \exp(-E/(RT)) \quad (4)$$

Thus higher temperatures and carbon concentrations $[C]$ shorten the induction time, whereas the variation of pressure in the range investigated had no effect on τ . At similar carbon concentrations and stoichiometry, τ is smaller for aromatic than for aliphatic hydrocarbons. The measured apparent activation energies, preexponential factors A and orders n are summarized in Table 1.

The maximum growth rate $(df_v/dt)_{max}$ of soot shows a typical bell-shaped curve when plotted versus temperature. The maximum is located at $T_m = 2000\text{ K}$ for the aromatic and 1800 K for the aliphatic hydrocarbons investigated. As indicated by the example (C_6H_6 , $\phi = 5$) in Fig. 4 higher carbon concentrations

TABLE 1
Parameters for Soot Growth from the Hydrocarbons Investigated

Exp. Conditions	Induction Time					$(df_V/dt)_{max}$		Growth Model	
	ϕ (-)	(C) (mol/m ³)	A [s ⁻¹ (mol/m ³) ⁻ⁿ]	n (-)	E (kJ/mol)	m (-)	T_m (K)	A_k (s ⁻¹)	E_k (kJ/mol)
Toluene	5	1–3	4.2×10^{10}	0.75	235	1.7	1970	1.6×10^8	170
Benzene	5	1–7	2.9×10^{10}	0.75	235	2.3	2010	1.4×10^8	170
Benzene	∞	1–7	2.9×10^{10}	0.75	235	2.1	1970	1.4×10^8	170
Acetylene	5	3–8	9.6×10^8	0.75	190	2.1	1770	—	—
Ethylene	5	3–9	2.6×10^8	1	190	2.2	1780	—	—
Propane	5	3–16	3.7×10^8	0.5	190	2.1	1770	—	—
n-Heptane	5	4–14	1.5×10^8	0.5	177	2.0	1780	—	—
Methane	5	3–14	5.3×10^7	0.24	160	2.0	1800	—	—

strongly increase the maximum soot growth rate. This can be described by: $(df_V/dt)_{max} \sim [C]^m$, with m being close to 2. The values of m are listed in Table 1 together with the temperatures T_m which give the maximum growth rates. We could not find any influence of the pressure on $(df_V/dt)_{max}$ when $[C]$ was kept constant. The bell-shaped curves were observed to drift with temperature for high carbon concentrations, where the impact of the reaction enthalpy on the bath gas temperature cannot be neglected anymore. At equal $[C]$ and stoichiometry, $(df_V/dt)_{max}$ is highest for benzene, followed by toluene, acetylene, and ethylene in turn. Next are propane and n-heptane, which give similar results. Soot growth is slowest for methane. Fuel-rich oxidation and pyrolysis experiments for benzene gave almost the same parameters (see Table 1). However, the amount of soot formed decreases strongly if the oxygen

content in the mixture is increased at constant carbon concentration.

The induction period and the maximum rate of soot growth are properties only of the early stage of soot formation. In Fig. 5, the soot volume fraction is plotted, for different reaction times against temperature; the maximum soot volume fraction is shifted to lower temperatures at increasing reaction times. In accordance with the results of $(df_V/dt)_{max}$, the maximum is located at 2000 K for short times. With longer reaction times, the measurements indicate a maximum lower than 1700 K; this is in good agreement with results obtained in premixed laminar flames. Experiments with high soot yields exhibit a remarkable decrease in the exponent s ($df_V/dt \sim [C]^s$) during growth. This

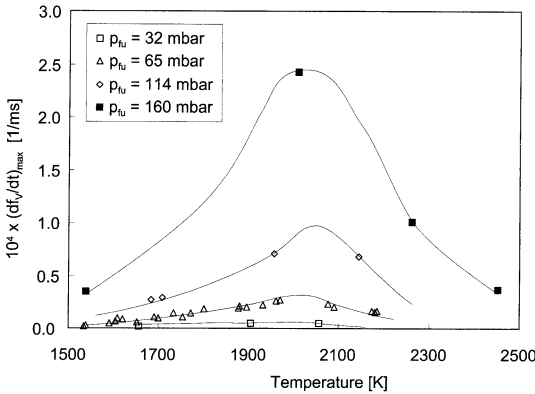


Fig. 4. Dependence of maximum soot growth on temperature and fuel partial pressure p_{fu} (C_6H_6 , $\phi = 5$).

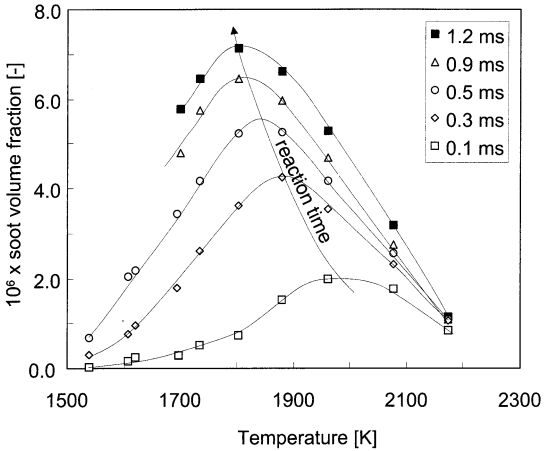


Fig. 5. Soot volume fraction f_V as a function of temperature for different reaction times (C_6H_6 , $\phi = 5$, $Ar = 99.5\%$, $p = 30$ bar).

can be explained by a lack of growth species due to the increasing fraction of carbon already converted into soot. Accordingly for enhanced $[C]$, the bell-shaped plot of $(df_V/dt)_{max}$ against temperature flattens around the maximum.

Growth Model

The development of the soot volume fraction following the point of maximum rate of soot growth can be represented by the first-order growth model [14]:

$$df_V/dt = k_f(f_{V,\infty} - f_V) \quad (5)$$

In this equation, k_f is the apparent rate constant and $f_{V,\infty}$ denotes the asymptotic soot volume fraction for long reaction times. The model parameters were determined for the aromatic hydrocarbons investigated; $f_{V,\infty}$ increases with carbon concentration and decreases with temperature but does not show a pronounced maximum with respect to temperature. The rate constants for benzene and toluene increase with temperature and can be expressed as $k_f = A_k \cdot \exp[-E_k/(RT)]$, with an apparent activation energy of $E_k = 170$ kJ/mol (see Table 1). This value is similar to results from premixed flames [4], indicating that the much discussed basic mechanisms for the decrease of soot growth rate with time are similar for both systems. Within the range of conditions investigated, no influence of pressure, carbon concentration, and stoichiometry on k_f was observed.

Experiments at temperatures higher than 2000 K were found to be dominated by a second growth stage, which follows the period of first-order growth. It is characterized by a nearly linear increase of f_V , starting when the soot volume fraction has almost reached the asymptotic value. This finding demonstrates that the growth law (Eq. 6) is not valid when f_V approaches $f_{V,\infty}$. Based on the fact that pressure does not affect the amount of soot formed, we conclude that all the important reactions take place in the high-pressure regime, and therefore are independent of pressure. Deviating from the results of others [5, 15] in this pressure range, we could not find any influence of pressure on soot volume fraction when $[C]$ was kept constant. It thus seems that these effects reported before have to be attributed to insufficient

mixing and the temperature increase produced by the exothermicity.

Particle Sizes and Number Densities

Most shock tube studies of soot formation have been restricted to the application of simple extinction techniques. However, the soot volume fractions determined by this method allow only a limited insight into soot formation. Time-resolved measurements of particle diameters and number densities provide a more detailed understanding of coagulation and surface growth. At present there is little knowledge on coagulation at high pressures, when particles change from free molecular flow to the transition regime. The uncertainty concerning soot particle growth behind the reflected shock at high pressures is reflected by the results published for the range of diameters from 40 nm to more than 200 nm [16, 17]. An analysis of the measurement techniques used in these experiments shows that the reliability of these values might be questionable [9]. Better results can be expected from the scattering method applied in the present work to determine particle sizes.

The evolution of the volumetric mean particle diameter d_V and the number density N , as obtained from the signals in Fig. 2, together with soot volume fraction and pressure are presented in Fig. 6. Similar to findings in flat flames, a fast initial increase of the particle diameter is observed, while the particle number density drops by orders of magnitude. This behavior reflects the process of coagulation accompanied by surface growth responsible for the rise in f_V . Low scattered signals and the steep increase of particle diameter both limit the quality of the measurements during initial particle growth. In addition, interpretation of the signals during this period is affected by PAH absorption. It is noticeable that N reaches almost a constant value after the first 3 ms. The drop of the number density of particles at $t = 3.2$ ms indicates the beginning of driver gas contamination in the measurement volume. Typical particle diameters determined in our experiments after a measurement time of 3 ms were in the range of 15 to 40 nm. The particle number densities measured are considerably higher than

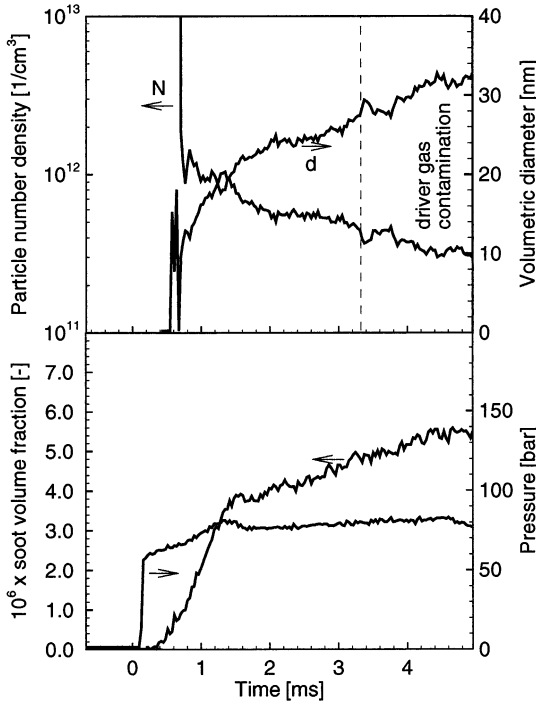


Fig. 6. Example of soot particle growth (C_7H_{16} , $\phi = 5$, $Ar = 99.5\%$, $T = 1820\text{ K}$, $p = 59.1\text{ bar}$).

typical values of $N \approx 10^{10}\text{ cm}^{-3}$ found in atmospheric-pressure flames.

The techniques applied offer the possibility of studying the effects of pressure, carbon concentration, and temperature on particle size and number density. Soot volume fractions, particle number densities, and particle diameters determined during partial oxidation of n-heptane ($\phi = 5$) at a temperature 1820 K are shown in Fig. 7. The values were determined 1.5 ms after detection of the first significant light scattering. In the case of constant carbon concentration (broken lines), an increase of pressure from 15 to 60 bar leads to slightly smaller particles and higher number densities. This effect is the expected result of slower coagulation: the pressure increase reduces the Knudsen numbers in the transition regime and results in decreased coagulation coefficients, i.e. slower coagulation. Experiments with constant argon dilution (solid lines) show the p^2 increase in f_V and a rise in soot particle diameter. However, the particle number density is enhanced together with f_V . This result differs from findings [18] at atmospheric conditions, where larger particles are

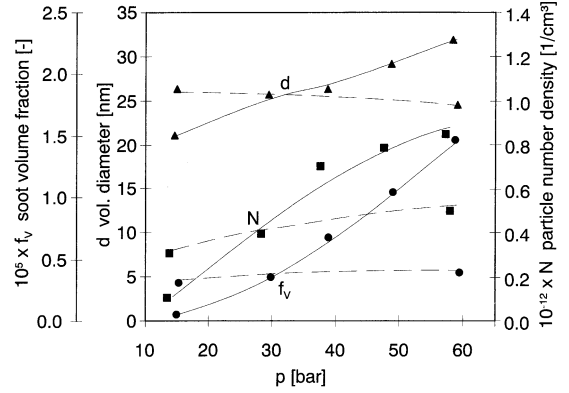


Fig. 7. Particle diameters, number densities, and soot volume fraction during oxidation of n-heptane ($\phi = 5$) taken 1.5 ms after the appearance of the first particles, $T = 1820\text{ K}$, solid: $Ar = 99.0\%$, dashed: $[C] = 4.3\text{ mol/cm}^3$.

observed with increased soot volume fractions; particle number densities, however, are only weakly affected. According to free molecular coagulation theory, for long reaction times N becomes proportional to $f_V^{-1/6}$ [18]. Hence, the high particle number densities observed in our experiments are the result of high pressures, together with elevated volume fractions. The results for aromatic hydrocarbons exhibit the same tendencies as for n-heptane. This is demonstrated in Fig. 8 for the oxidation of toluene ($\phi = 5$). Again the increase of pressure and corresponding rise of carbon concentration leads to larger particles and higher number densities. When plotted versus temperature, it is apparent that both f_V and N exhibit a bell-shaped curve (Fig. 9). This finding confirms the strong coupling between the two quantities shown in Figs. 7 and 8. The comparison at equal

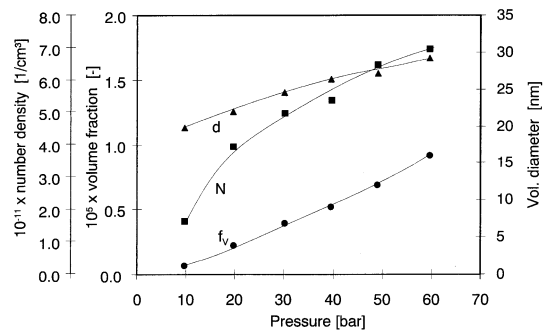


Fig. 8. Pressure dependence of particle diameter, number density, and soot volume fraction in oxidation of toluene $\phi = 5$, $T = 1600\text{ K}$, $Ar = 99.75\%$.

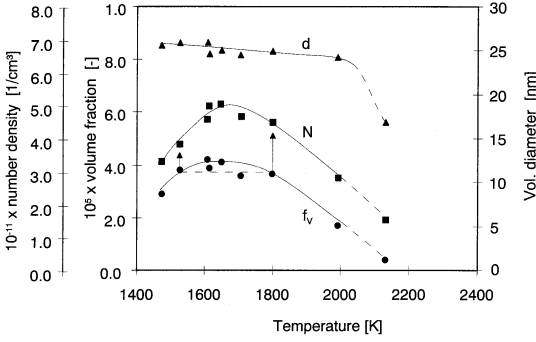


Fig. 9. Temperature dependence of particle diameter, number density, and soot volume fraction in oxidation of toluene $\phi = 5$, $p = 30$ var, Ar = 99.75%.

f_v at the left and the right side of the f_v -maximum reveals larger number densities on the high temperature side. Coagulation seems to be slowed down earlier in this temperature region. Particle diameters were found to increase if the temperature was lowered. This tendency is in agreement with measurements from benzene pyrolysis in a flow reactor by Prado et al. [18].

Particles deposited on carbon grids attached to the shock tube wall were extracted from the tube after the experiment and analyzed by TEM. The primary particle diameters follow the same tendencies as the results from the optical measurements. However, the TEM particle sizes are smaller; this has to be attributed to aggregation during our experiments. Based on the assumption that the diameter of the equivalent sphere is determined by the scattering technique, the number of primary particles per aggregate can be estimated to be ~ 5 , so only small aggregates are present.

Analysis of Soot Particle Coagulation

The results presented above show the influence of reaction parameters on particle sizes and number densities. To obtain a deeper insight into soot particle growth at high pressures we have compared the observed particle growth with theoretical calculations on coagulation. For this analysis, the coagulation equations were solved in discrete form by an in-house aerosol dynamics code. The first term of

$$\left(\frac{dN_n}{dt}\right)_{coag} = \frac{1}{2} \cdot \sum_{j=1, n=j+i}^{n-1} C_{ij} \cdot b_{ij} \cdot N_i \cdot N_j - N_n \cdot \sum_{i=1}^k C_{in} \cdot b_{in} \cdot N_i \quad (6)$$

describes the formation and the second term the consumption of particles of size n . The semi-empirical expression by Fuchs [19] was used to determine the coagulation coefficients b_{ij} between spherical particles of size class i and j . N denotes number density and C the van-der-Waals (vdW) enhancement factor. In all, 150 classes of particles were used in the calculations; this was found to be a good compromise between CPU time and the desired accuracy. When the particles grow, their diameter increases to values comparable to the mean free path of the gas; so there is a change from the free molecular to the transition regime. Here the coagulation coefficients decrease and become less dependent on the particle diameter. At high pressures special emphasis has to be put on the incorporation of dispersion forces into the coagulation equation; the attractive forces increase the probability of collisions. In contrast to the free molecule regime, the vdW enhancement cannot be represented by a constant factor, but depends on pressure, particle size, and temperature. It has been calculated following a strategy suggested by Kennedy [20]. The retarded vdW enhancement factors are obtained by approximating the interaction energy of spheres by the product of an exact retarded Hamaker constant for planar half-spaces with a Hamaker geometrical factor to account for the sphericity of the particles [21]. With increasing pressure and particle size, C_{ij} is reduced. The code has been validated with Harris and Kennedy's calculations [22], which simulate the coagulation of an initially monodisperse aerosol undergoing coagulation at high pressure; good agreement has been achieved.

To illustrate the effects of pressure and soot volume fraction on particle growth, we have performed calculations for constant f_v . The results are presented in Fig. 10. At atmospheric pressure an increased soot volume fraction leads to larger particles. These enhance coagulation and cause decreased number densities.

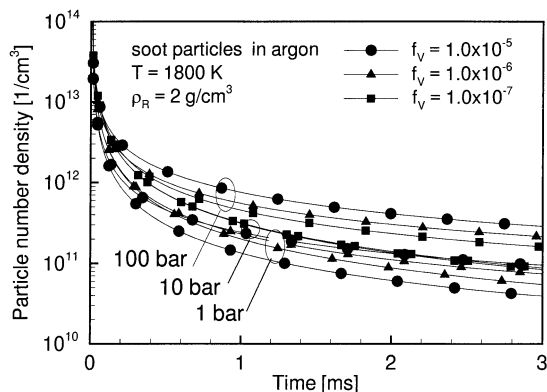


Fig. 10. Simulated evolution of particle number density as a function of pressure and soot volume fraction.

Obviously with rising pressure the effect is reversed and N scales with f_v . Two reasons are responsible for this phenomenon: at high pressure the particles quickly reach a size where b_{ij} becomes almost independent of particle diameter. Secondly, at high pressure the vdW enhancement decreases strongly with particle size and leads to reduced coagulation and higher particle number densities. This behavior is expressed by the bell-shaped plots of N versus temperature observed in our experiments.

At high Knudsen numbers, the calculated particle size distribution of a coagulating aerosol moves towards the self-preserving form. At high pressures and soot volume fractions, as an increasing fraction of the size distribution shifts from the free molecular to the transition regime, the size distribution narrows due to reduced coagulation coefficients and enhancement factors for the larger particles of the distribution. This has to be considered when comparing the calculations with experimental results as the shape of the distribution is essential for the determination of the particle number densities from optical measurements. A size distribution obtained from TEM at the end of the experiment is not representative of the early particle growth and can induce errors in N of 40%. To examine the influence of aggregation on coagulation at high pressures, we have applied different models suggested [23, 24] for aggregation in our calculations. All the results indicate that the formation of aggregates, which can strongly enhance coagulation in the free molecular regime, has only a minor impact on particle

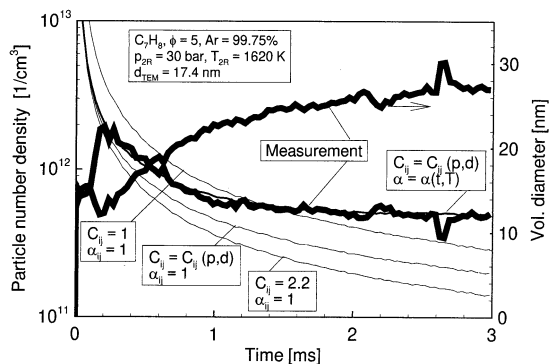


Fig. 11. Particle coagulation at high pressures: example of measured and calculated particle number densities (C_7H_8 , $\phi = 5$, $Ar = 99.75\%$, $p = 30$ bar, $T = 1610$ K). ($C_{ij} = 1$, $\alpha = 1$) neglected vdW forces, ($C_{ij} = 2.2$, $\alpha = 1$) constant vdW enhancement factor, [$C_{ij} = C(p, d)$, $\alpha = 1$] enhancement factors as a function of pressure and particle size, $C = C(p, d)$ with reduced sticking efficiency $\alpha_{ij} = \alpha(t, T)$ (Eq. 8).

number densities in the transition regime. It was therefore neglected in subsequent calculations.

The next step was to compare the measured rates of particle growth directly with the results from simulations with the aerosol code. Detailed chemical mechanisms for toluene and n-heptane including soot formation are presently not available for our experimental conditions. As the main focus of our experiments was to study coagulation, the following strategy was adopted to compare simulated and measured rates of particle growth: the nucleation rate was calculated from the light absorption at the point when the first particles were detected. The nucleating particles were assumed to be monodisperse with a diameter of 1 nm. Their particle number density was derived applying the Rayleigh-approximation. The surface growth rates were taken from the experiment presuming the growth rate to be proportional to the particles' surface area.

Figure 11 shows a typical example of the measured particle diameter and number density, together with calculated number densities. The volumetric mean diameter obtained by TEM after the experiment was 17.4 nm. Assuming that every collision of particles leads to coagulation ($\alpha = 1$), no satisfactory agreement can be found between simulation and experiment. If dispersion forces are not considered ($C_{ij} = 1$), initial coagulation is clearly underestimated, whereas the value of $C_{ij} = 2.2$,

which is often applied in the free molecule regime, overestimates the rate of coagulation. If the pressure and size dependence is taken into account, the coagulation coefficients are reduced during particle growth. Close agreement, however, can only be observed during the first 1 ms of particle growth. At longer times measured coagulation rates are much smaller than predicted from the simulation. A look at the measured surface growth rates reveals that they have also dropped significantly, indicating that the particles have strongly reduced their surface reactivity [25]. Two possible explanations for the disagreement between measured and calculated rates of coagulation have to be taken into consideration: incorrect interpretation of the optical measurements, and insufficient description of the particle coagulation in our model. Both aspects have been investigated.

A detailed analysis of our measurement technique included the effects of incorrect assumptions about the refractive index, the size distribution, and particles deviating from a spherical shape. It was found that the reported variations of the refractive index [11] with the position in the flame cannot be responsible for the observed effect. Further, a strong reduction of the width of the size distribution would induce high number densities for the particles. However, there is no evidence of such behavior in the calculated size distributions or in our TEM results. Soot agglomerates in chainlike structure, which are composed of nearly spherical particles of equal size. They can be described by the fractal-like relationship

$$n = k_f \left(\frac{R_g}{d_p} \right)^{D_f} \quad (7)$$

where n is the number of primary particles in an aggregate, d_p is the primary particle diameter, R_g the radius of gyration of the aggregate, D_f the fractal dimension, and k_f the fractal prefactor. There is large agreement that D_f for soot particles is between 1.6 and 1.9; k_f is more difficult to obtain from measurements, as its determination requires the three-dimensional structure of the aggregate. Results from aggregation simulations suggest a value of 5.8 [26], whereas measurements in flames gave $k_f = 8.5$ [27].

If the Rayleigh approximation is applied to analyze scattering measurements, the particle diameter is obtained as a function of Q_{VV}/k_{ext} (see

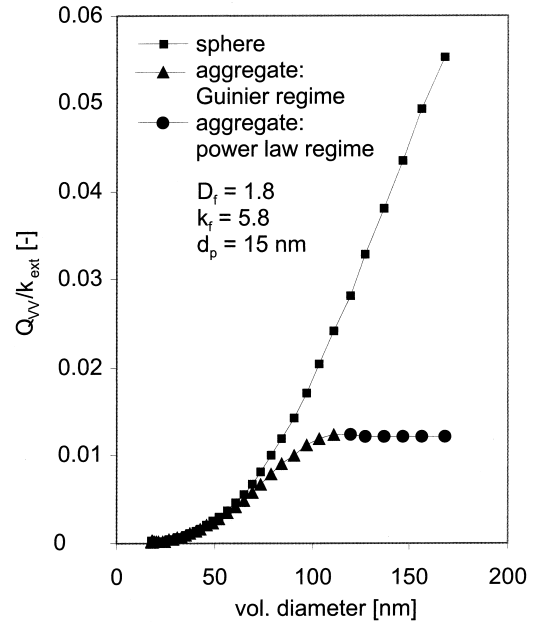


Fig. 12. Optical properties of an aggregate with monodisperse primary particles of 15 nm diameter ($D_f = 1.8$, $k_f = 5.8$) and a sphere of equal volume.

Eqs. 2 and 3). A common approach to describe the optical properties of aggregates is the Rayleigh-Debye-Gans approximation [28]. An example of aggregate optical properties calculated with this method is given in Fig. 12. It shows Q_{VV}/k_{ext} plotted against aggregate size for $D_f = 1.8$ and $k_f = 5.8$ assuming monodisperse primary particles with 15 nm diameter. The plot reveals that once particles reach the power law regime, the measured particle size will become independent of the volumetric diameter of the aggregate. This underestimation of the particle size would lead to an overestimation of particle number density, as observed in our experiments.

Enhanced particle number densities have also been found in high-pressure flames with pressures up to 15 bar. The dissociation of agglomerated, deactivated particles has been proposed as an explanation [2, 3]. Recently a detailed model was used [29] to simulate soot growth and coagulation in these flames. The method of moments including coagulation in the transition and continuum regime and formation of aggregates was applied. The authors claimed [29] reduced scattering due to aggregates in the power law regime to be the cause of the apparent high particle number densities. They used $k_f = 4.3$,

which is at the lower limit of reported values. Decreasing values of k_f shift the crossover between the two regimes to smaller particles.

The example in Fig. 12 shows that strong differences between spherical and aggregate scattering occur only for volumetric particles' diameters larger than 60 nm. Considering the primary particle sizes obtained by TEM (15–22 nm) and our optically determined volumetric diameters (<40 nm), agreement between simulations and measurements can be only obtained assuming a very small value of k_f , which has to be much lower than the values reported in literature. Hence, aggregation does not seem to be responsible for the enhanced particle number densities. However, aggregates resulting from high-pressure soot formation have not been analyzed for their aggregate structure. Simulations of aggregate growth and structure at high pressure would be very helpful for interpreting optical soot measurements in high-pressure environments.

The dispersion forces in the calculation include only the attractive vdW potential. Not considered are the repulsive forces and the kinetic energies of the particles and the gas molecules. These may reduce coagulation once chemical bonds lose their dominance in holding the particles together. The effect of a sticking efficiency α lower than unity for particle collisions has been addressed theoretically [30]; in fact, it has been shown that unsuccessful collisions in the free molecule region are dominant for particles with diameters less than 5 nm. However, calculations for soot particles in the transition regime at high temperatures have not been performed yet.

In the absence of theoretical predictions for α_{ij} we have developed an empirical correlation for the mean sticking efficiency α , whose use gives agreement between calculation and experiment. In contrast to the free molecule regime at lower Knudsen numbers the proportionality between b_{ij} and α_{ij} is cancelled and α_{ij} loses influence. Generally, we observed a fast decrease of the coagulator rates with reaction time and very low dN/dt at long times. Consequently, the following formula

$$\alpha = \exp(-t_P k_r) \quad (8)$$

was applied to describe α as a function of particle life time t_P : Eq. 8 reduces α from 1

(perfect sticking) to 0 (no coagulation) for a rate constant k_r . To determine k_r we compared experiments and simulations using the measured temperatures and pressures. The calculated $\langle d^6 \rangle / \langle d^3 \rangle^2$ was considered in the interpretation of our scattering measurements. It was found that k_r increases with temperature and reaches a maximum at 1900 K and or then decreases again. No significant influence of pressure or carbon concentration on k_r could be observed. Hence the following correlation for the sticking efficiency has been established:

$$k_r = 2.0 \times 10^3 \exp \left\{ -\frac{(1900 - T)^2}{(260)^2} \right\} [s^{-1}] \quad (9)$$

This was found to match the results of experiments with toluene and n-heptane in the temperature range investigated. It confirms that the primary fuel is only of minor importance to the process of coagulation. The calculation performed for the example in Fig. 11 shows good agreement with experiment [$C_{ij} = C_{ij}(p, d)$, $\alpha = \alpha(t, T)$].

We would expect α to depend strongly on particle size, which should influence the evolution of the particle size distribution. However, the determination of the size dependence of α seems to be very difficult in experiments. Detailed numerical simulations of collisions between particles may be the key to a deeper understanding of soot particle coagulation at high pressures and also to a physical explanation of the observed phenomena.

CONCLUSIONS

Soot growth from different aliphatic and aromatic hydrocarbons has been characterized with respect to the induction period and the maximum rate of soot growth. The parameters of a growth model were determined for toluene and benzene. The apparent activation energy of the rate constant k_f is in good agreement with results from experiments with flames.

Soot volume fraction has been found to be strongly dependent on temperature and carbon concentration. Pressure has no effect on soot mass growth in the pressure range investigated.

Using a light scattering technique, optical measurements of particle sizes and number densities

in the reflected shock region were performed. High particle number densities have been found; also they increase with soot volume fraction. Particle diameters between 15 and 40 nm were detected. The comparison with measurements from TEM indicates that the particles are aggregates consisting of a few primary particles.

Our simulations of particle growth show an increase of particle number density with enhanced soot volume fraction. This phenomenon is the opposite of what is observed under atmospheric conditions.

Measured and calculated rates of coagulation agree well during early particle growth. When particle reactivity decreases, strongly reduced coagulation rates are found, leading to high particle number densities. Two approaches to explain this have been discussed: the influence of aggregation on scattering measurements and reduced sticking efficiencies during coagulation. Both may contribute to the effect; however, our knowledge is too limited to allow a final assessment. More experiments and additional numerical simulations of particle collisions, aggregate growth, and structure at high pressure will give a better insight into this effect.

The results of this study indicate that in emissions of jet and diesel engines the particle diameters are smaller and particle number densities may be significantly higher than expected from theoretical estimations. This should be considered in studies on the effect of soot particles on human health and atmospheric processes.

This research program has been supported by the Deutsche Forschungsgemeinschaft within the scope of the Graduiertenkolleg "Energie- und Umwelttechnik."

REFERENCES

1. Böhm, H., Hesse, D., Jander, H., Lüers, B., Pietscher, J., Wagner, H. G., and Weiss, M., *Twenty-Second Symposium (International) on Combustion*, The Combustion Institute, Pittsburgh, 1988, p. 403.
2. Böhm, H., Feldermann, C., Heidermann, T., Jander, H., Lüers, B., and Wagner, H. G., *Twenty-Fourth Symposium (International) on Combustion*, The Combustion Institute, Pittsburgh, 1992, p. 991.
3. Hanisch, S., Jander, H., Pape, T., and Wagner, H. G., *Twenty-Fifth Symposium (International) on Combustion*, The Combustion Institute, Pittsburgh, 1994, p. 577.
4. Wagner, H. G., *AGARD Conference Proc. No. 422*, 1988, p. 24-1.
5. Bauerle, S., Karasevich, Y., Slavov, S., Tanke, D., Tappe, M., Thienel, T., and Wagner, H. G., *Twenty-Fifth Symposium (International) on Combustion*, The Combustion Institute, Pittsburgh, 1994, p. 627.
6. Graham, S. C., *Sixteenth Symposium (International) on Combustion*, 1976, p. 663.
7. Stasio, S., and Massoli, P., *Combust. Sci. Technol.* 124:219 (1997).
8. Kellerer, H., Müller, A., Bauer, H.-J., and Wittig, S., *Combust. Sci. Technol.* 113:67 (1996).
9. Kellerer, H., Bauer, H.-J., and Wittig, S., *Twentieth International Symposium on Shock Waves*, 1996, p. 947.
10. d'Alessio, A., Beretta, F., Cavalliere, A., and Menna, P., *Soot in Combustion Systems and Its Toxic Properties*, Plenum, New York, 1983, p. 355.
11. Charalampopoulos, T. T., and Chang, H., *Combust. Sci. Technol.* 59:401 (1988).
12. Lee, S. C., and Tien, C. L., *Eighteenth Symposium (International) on Combustion*, The Combustion Institute, Pittsburgh, 1980, p. 1159.
13. Tsuboi, T., and Nagaya, K., *Sixteenth Symposium on Shock Tubes and Shock Waves*, Springer, 1987, p. 503.
14. Haynes, B. S., and Wagner, H. G., *Prog. Energy Combust. Sci.* 7:229 (1981).
15. Müller, A., and Wittig, S., *Eighteenth International Symposium on Shock Waves*, 1991, p. 759.
16. Yao, J., Fieweger, K., Kleppel, M., and Adomeit, G., *Nineteenth International Symposium on Shock Waves*, World Scientific, Singapore, 1996, p. 167.
17. Parker, T. E., Foutter, R. R., and Rawlins, W. T., *Seventeenth Symposium on Shock Tubes and Shock Waves*, 1989, p. 481.
18. Prado, G., Lahaye, J., and Haynes, B. S., *Combustion Systems and Its Toxic Properties*, Plenum, New York, 1983, p. 145.
19. Fuchs, N. A., *The Mechanics of Aerosols*, Pergamon Press, Oxford, 1964.
20. Kennedy, I. M., *Combust. Flame* 68:1 (1987).
21. Pailthorpe, B. A., and Russel, W. B., *J. Coll. Interf. Sci.* 89:563 (1982).
22. Harris, S. J., and Kennedy, I. M., *Combust. Flame* 78:390 (1989).
23. Wu, M. K., and Friedlander, S. K., *J. Aerosol Sci.* 23:71 (1992).
24. Xiong, Y., and Pratsinis, S. E., *J. Aerosol Sci.* 24:282 (1993).
25. Kellerer, H., and Wittig, S., *Twenty-First International Symposium on Shock Waves*, Pather, Fyshwick, 1997, p. 177.
26. Mountain, R. D., and Mulholland, G. W., *Langmuir* 4:1321 (1988).
27. Köylü, Ü. Ö., Faeth, G. M., Farias, T. L., and Carvalho, M. G., *Combust. Flame* 100:621 (1995).
28. Dobbins, R. A., and Megaridis, C. M. (1990). Second International Congress on Optical Particle Sizing.
29. Kazakov, A., and Frenklach, M., *Combust. Flame* 112:270 (1998).
30. Narsimhan, G., and Ruckenstein, E., *J. Coll. Interf. Sci.* 107:174 (1985).

Received 6 July 1998; revised 22 February 1999; accepted 25 April 1999